Numerical investigation on Blade-Wake Interaction noise. Toward a better understanding of BWI mechanisms.

Yann Mauffrey, Gilles Rahier, Jean Prieur

ONERA, BP 72, 92322 CHATILLON Cedex, France
Tel : 33 1 46734752, Fax :33 1 46734166

yann.mauffrey@onera.fr, gilles.rahier@onera.fr, jean.prieur@onera.fr

32nd European Rotorcraft Forum, 12-14 September 2006

Abstract. The capability of short wave instabilities developing near rotor tip vortex cores of being the main source of BWI noise is investigated. In this aim, a numerical simulation of these instabilities is performed considering a simplified wake geometry. The aerodynamic fields are extracted to determine the blade pressure response using unsteady compressible airfoil theory. Finally a loading noise computation is performed. All the results obtained from these computations are compared to HART II experimental data and a good qualitative agreement is found.

1 INTRODUCTION

Blade-Wake Interaction (BWI) has been recognized as a significant component of main rotor noise pollution particularly in flight conditions where Blade Vortex Interaction noise (BVI) is less intense like climb or level flight. For these flight conditions, BWI is a more important source of noise in terms of intensity than BVI (climb) or equivalent to BVI (level flight). Blade-Wake Interaction is characterized by broadband noise located in an intermediate frequency domain between BVI and turboshaft engine noise (typically 1 to 3 KHz full scale).
This noise was initially identified by Brooks [1]. Analysing experimental acoustic spectra, Brooks connected BWI noise to non-periodic blade pressure fluctuations in the mid-frequency range. Dealing with this idea, Brezillon [2] analysing blade pressure measurements performed during HART wind tunnel test [3], tried to establish a relationship between these broadband pressure fluctuations and the blade wake. He compared mid-frequency blade pressure perturbation azimuthal occurences on the rotor disk with close BVI events using a free wake BVI prediction code. This comparison permitted to associate BWI sources with perpendicular blade vortex interactions. These interactions concern vortices whose age is less than 180 degrees. Glegg[4] tried to build a BWI prediction model assuming that the noise was resulting from interactions between the blades and isotropic homogeneous turbulence contained in tip vortices. First results indicated that the turbulent kinetic energy contained in an isolated vortex is not sufficient to account for BWI noise levels. This finding brought Wittmer [5] to search for alternative mechanisms of turbulence production inside rectilinear vortices. He showed that the turbulent zones around vortices were larger when they had already interacted with a blade. Modifying his prediction model consequently, Glegg [6] obtained noise levels in agreement with experimental data. Contrary to [4], analysis of experimental blade-pressures in [2] tended to show that contributions of tip vortices who did not previously interact with a blade, are comparable to that of vortices having already encountered a blade.
A thorough analysis by Bouchet [7] of the same HART experimental blade pressures as in [2] demonstrated that BWI was not related to isotropic turbulence but rather the result of blade interactions with coherent large-scale structures present in the flow. Moreover he linked these structures to short-wave vortex instabilities.
This kind of instabilities occurs when an external strain field elliptically deforms the vortex

core. Then the deformation permits the resonant coupling of two modes (Kelvin modes) of the vortex.
Observing that BWI pressure fluctuations occur at azimuths where the blade interacts with two close tip-vortices, Bouchet laid the hypothesis that elliptic instabilities of co-rotative vortex pairs were the source of BWI. Readers can refer to Le Dizes [8] for linear analytical study and Laporte [9] for numerical study of this kind of instabilities.
This paper aims at verifying, using numerical simulations, that short-wave instabilities developing near tip vortex cores could be a source of BWI. A climb flight condition is chosen. Since a full-rotor computation is not presently feasible because the number of points needed would be prohibitive as regards to the characteristic dimensions of the instabilities structures, another way is followed.
First, we evaluate the capability of the CFD code *elsA* [10] to simulate the development of vortex elliptical instabilities. Then a numerical simulation is performed for a pair of rectilinear, uniform and parallel vortices on a limited domain.
The velocity perturbations issued from the computation are then used to determine the blade pressure fluctuations generated by the blade/vortex instability encounter. To perform the prediction of the blade aerodynamic response to this perturbation field, Amiet's theory [11] is employed.
Eventually, these blade pressure perturbations serve as input data to a loading noise computation performed using the PARIS [12] code. The acoustic computation is based on an integral formulation of Ffowcs Williams and Hawkings equation solution.
At each step, the results are compared to HART II [13] experimental data and discussed.

2 NUMERICAL SIMULATION OF SHORT WAVE INSTABILITIES

2.1 Geometrical characteristics of tip-vortices

In this section we present the geometrical characteristics of the problem and we describe the vortex short wave instabilities which can be induced in this configuration.

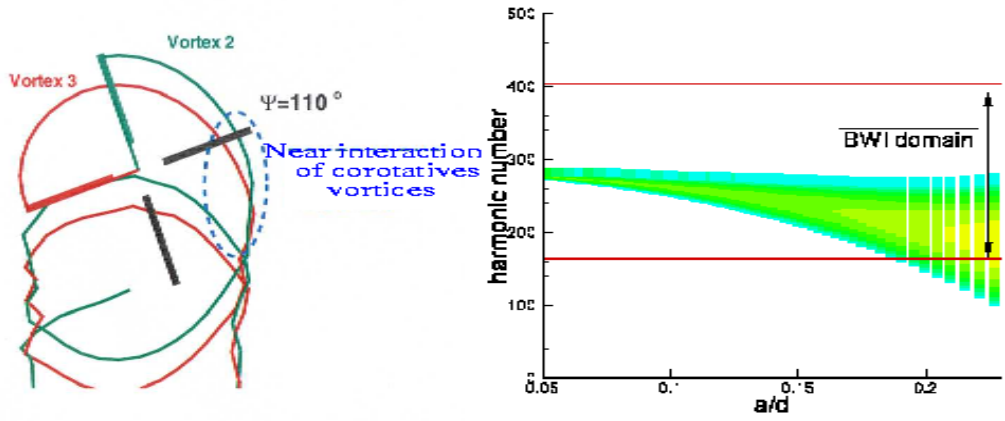

Figure 1: left :wake configuration in the case of climb flight. right : Frequency domain of short wave instabilities against a/d ratio. Colour scale : The instability growth rate increases from green to yellow

Figure 1 left side shows tip vortex position in a climbing flight configuration. Particular

attention should be drawn to the vortex conformation in the BWI occurrence zone ($\Psi = 110°$). We can see a close interaction between the two tip vortices at this azimuth. This interaction could make possible the development of short-wave instabilities also called elliptic instabilities on each vortex. Figure 1 right side presents the frequency domain for the first branch of elliptical instability of a Lamb-Oseen like vortex profile. The frequency domain is plotted as a function of the ratio a/d (where a is the vortex core-size, and d the separation distance between the two vortices). This result is issued from the linear study of Le Dizes. One can observe that the frequency domain of instabilities is in the frequency range of BWI centered about 250 times the rotor rotation frequency.

It also clearly appears that the ratio a/d has a major influence on elliptical instabilities : The closer the vortices the higher the instability growth rate and the larger the instability frequency range. The spatial extent of the instability also depends on this ratio. The instability originates near each vortex centre and extends further to its periphery as the ratio a/d increases. This latter phenomenon is caused by the saturation of the short-wave instability at small amplitudes and in the case of small a/d ratio.

Thus to pursue the discussion on the type of instabilities that can occur, one needs to have an estimation of a/d. A Free wake computation together with a physical model of the core size evolution was employed for this purpose. With this method an average ratio a/d = 0.10 was obtained in the main azimuthal range of BWI : [90°-120°].This ratio appears to be in a middle range and is sufficient to spawn elliptical instabilities which thus appear as a possible BWI source. It should also be noticed that the medium value of a/d implies that the instability remains confined in the vortex vicinity. As a consequence, one can consider the evolution of the instability occurring on one vortex independently of the other.

Remark: More generally, short waves instabilities can occur when a vortex experiences an external strain field which elliptically deforms its core. The strain field induced by the rotor wake on the tip-vortices could thus also be source of instability. It could explain experimental pressure fluctuations associated to BWI that appear at azimuths where the distance between vortices is larger.

2.2 Numerical set up.

An Euler numerical simulation is performed. Actually viscosity is assumed to have a weak influence in the first steps of instability development.

The numerical tool used to simulate the two dimensional as well as the three dimensional dynamics of the two-vortex flows is the ONERA finite volume Navier-Stokes solver *elsA*. This solver works on structured meshes. The simulations are performed using a fourth order explicit Runge-Kutta method for the time integration. The advective terms are discretised with a second order Jameson skew symmetric centred scheme. No second order dissipation is imposed and the fourth order dissipation term is set to have minimum diffusion. Concerning the boundaries, periodic conditions are applied on the domain edges cutting the vortices and far-field conditions are applied on the other domain boundaries.

The mesh is locally refined in cross-flow planes in the region of the two vortices, so as to obtain 10 points in the vortex core radius. In this direction, the boundaries are far from the vortex pair (distance between the centre of the domain and boundaries of the order of 10 times the initial vortex separation distance). In these planes the total number of points is 47961. For the first step of this study consisting in a comparison of computed instability growth rate with theoretical ones obtained by Le Dizes from linear analysis, the mesh size in the axial direction is set equal to the wavelength we want to simulate. A discretisation of 20 points per wavelength is chosen.

The flow is composed of a pair of parallel rectilinear and uniform corotative vortices centred in the cross flow direction as regards to the computation domain. The two vortices have the same circulation. We choose Lamb Oseen like vortex velocity profiles. In a cylindrical coordinate system (r, θ), the definitions of velocity and pressure relative to this profile write :

$$\begin{cases} V_r = 0 \\ V_\theta = \dfrac{\Gamma}{2\pi r}\left(1 - e^{-\frac{r^2}{a_o^2}}\right) \\ \dfrac{dP}{dr} = \rho \dfrac{v_\theta^2}{r} \end{cases} \tag{2.1}$$

Where Γ is the circulation, a_0 is the viscous core radius, ρ the density. This tangential velocity profile has been compared by Han [14] to experimental LDV measurement, and has been found an acceptable approximation. No experimental results were found in literature about axial velocity profile in climbing flight conditions. Experimental results of Mc Alister [15] and Han from PIV and LDV measurements on a hovering rotor gave a ratio between maximum tangential velocity and axial velocity greater than 5. Laporte showed that for this ratio the axial velocity has a weak influence on the instability modes developing inside the vortices. Moreover the axial velocity does not play a dominant part in the determination of the acoustic sources. Consequently, the axial velocity deficit is not taken into account. The three dimensional computation is set as follows :

- Initial conditions are given by a preliminary 2D computation. The linear superposition of two Lamb Oseen vortex aerodynamic fields is not solution of Euler equations. This fact could introduce an error for the 3D instability computation. Indeed, the linear superposition is introduced as the initial condition of a 2D computation. During the simulation, the strain field induced by one vortex on the other elliptically deforms the other vortex core and the vortex system begins to rotate at an angular velocity $\Omega_o = \dfrac{\Gamma}{\pi d^2}$. This simulation is performed until a stationary solution is reached.
- The aerodynamic solūtion obtained is then introduced by extending the velocity, pressure, and density fields in the third dimension and perturbing the velocity fields by a white noise. If (u_0, v_o, w_o) is the unperturbed velocity field at each mesh point, the white noise is introduced as follows: let r be a random number in the range $[-0.5\,10^{-3}; 0.5\,10^{-3}]$ thus :

$$\begin{cases} u = u_0(1+r) \\ v = v_0(1+r) \\ w = 0 \end{cases} \tag{2.2}$$

In the following, we will only take into account the results until the start of the non-linear amplification regime.

2.3 Results.

Three dimensional elliptic instability results in a sinusoidal deformation in the vortex axial direction. Le Dizes, in the context of linear instability theory, gave an analytical approximation of the instability growth rate as a function of the vortex pair characteristics. In order to evaluate the *elsA* aerodynamic code to simulate the development of the instability, series of calculations was carried out by privileging a wavelength. Circulation Γ and viscous core radius a_0 are deduced from results of the ONERA BVI computation chain [16] for HART II mild climb flight configuration. We found : $\Gamma = 4.7\mathrm{m}^2 s^{-1}$, $a_0 = 1.68\mathrm{cm}$. The instability development inside vortices is presented below :

- A linear amplification phase where Kinetic energy E_k associated to only one

wavelength exponentially grows as $E_k(t)=E_k(0)e^{\sigma t}$ with t the time and σ the growth rate.

- A weakly non-linear regime of instability development then occurs. This regimes means that sub-harmonics of the fundamental mode are amplified.
- At last a non linear regime occurs. This regime corresponds to the amplification of all the modes computed. In our study, due to the weak ratio a/d, we observe a non-linear saturation of the instability at a short amplitude. Sipp [17], in the context of weakly non-linear analysis of a contra-rotative vortex pair instability, shows that as the ratio a/d increases, the amplitude of instability saturation is greater. In our case if Δ is the vortex centre displacement in the axial direction (located as the vorticity maximum) we obtain $\Delta/d=0.0097\mp0.00175$ which is quite in good agreement with Sipp's predictions.

The linear and weakly non-linear regime of the elliptical instability has to be interpreted as a transition to turbulence regime. The non-linear regime could thus be interpreted as a turbulent phenomena. This could be connected to a production mechanism of anisotropic turbulence in the vortex periphery.

Figure 2 shows the comparison between theoretical evolution of the amplified mode predicted by Le Dizes and evolution of kinetic energy perturbation related to the amplified mode in linear regime found by the present simulation for two different values of wavelength λ. The evolution of the amplitude of the instability mode is obtained by the following procedure. At each time of the simulation the instantaneous kinetic energy associated to a single vortex, same at every time step, is averaged over each orthoaxial planes of the simulation domain. We thus obtain a kinetic energy according to the axial direction of the vortex. The square root of this kinetic energy is then decomposed into axial Fourier modes. Finally the growth rate of the instability is obtained from the time evolution of the most amplified mode.

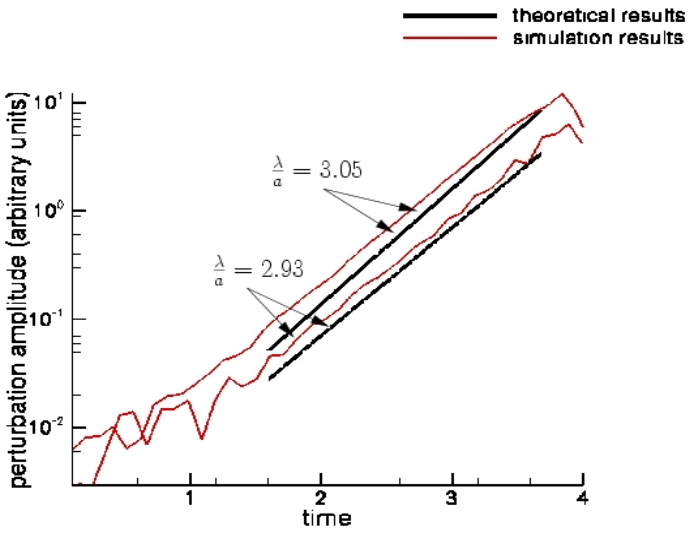

Figure 2:Theoretical [8] and present numerical simulation comparison of the time-amplification mode in the linear regime of elliptic instability. (Time is normalised by the rotor revolution period)

One can notice that on Figure 2 the growth rate obtained from simulation is close to the one predicted by Le Dizes. A difference of 7% for the wavelength $\lambda/a=3.05$ and less than 2% for $\lambda/a=2.93$ is observed. One can see that the time necessary to the development of instability does not correspond to the hypothesis of an interaction of the blade with vortices having 180

degrees maximum of age. This dissension could be due to the fact that, contrary to the numerically simulated configuration, actual tip-vortices are neither rectilinear nor parallel. Moreover, effective tip vortex velocity profiles are not axisymmetric as the vortex analytical model we have considered. A study of the frequency range and growth rate of the instability in more realistic configuration will belong to a future work.
Nevertheless, this simulation in a simplified configuration allows a first analysis of the phenomenon and potential sources of noise that these instabilities can create. This acoustic aspect is developed in the following section.

3 ACOUSTIC ANALYSIS

In this part we search to evaluate the acoustic consequences of perpendicular blade-perturbed vortices interactions in the context of helicopter rotor flow. In this optic, we evaluate the pressure fluctuations that normal perturbations of the velocity field would generate on a blade by extracting information from a selected plane of the 3D CFD computation and evaluate the pressure jump perturbation on the blade from Amiet's compressible gust airfoil theory. Then a loading noise prediction is performed starting from these pressure jump time histories.

3.1 Determination of the gust.

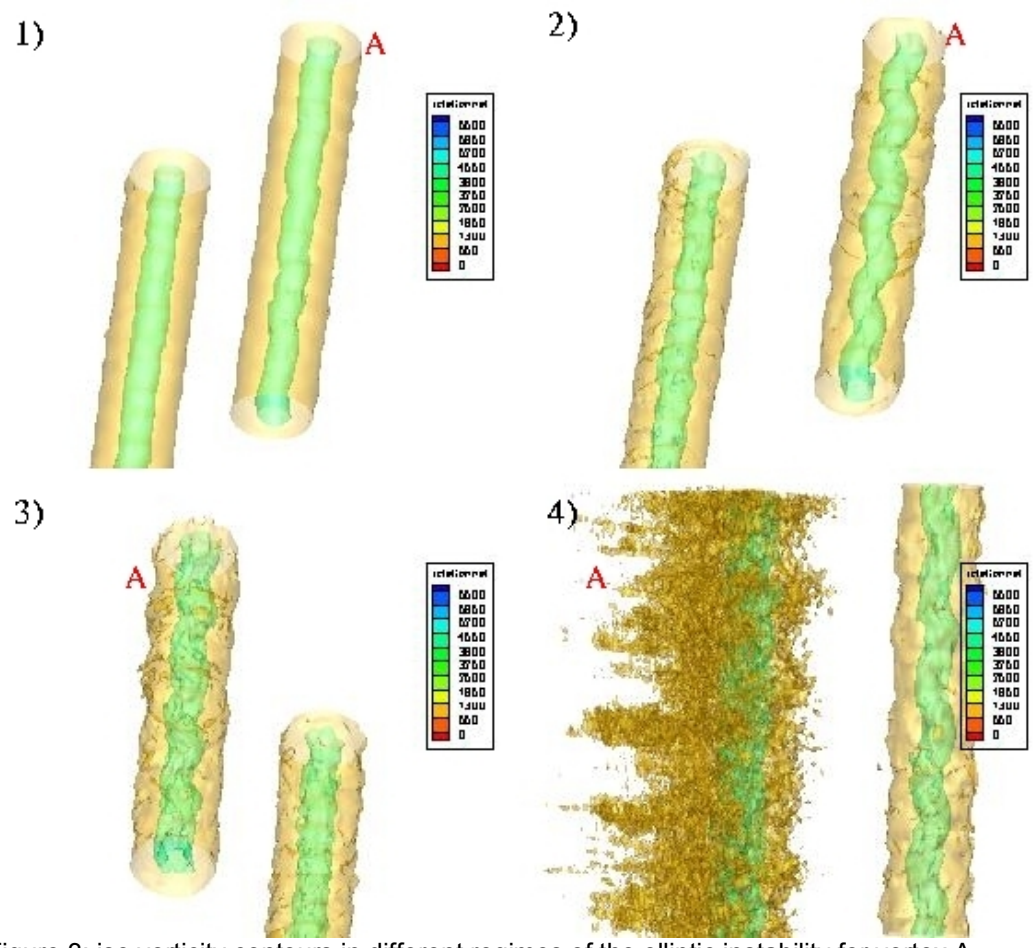

Figure 3: iso vorticity contours in different regimes of the elliptic instability for vortex A

The numerical simulation of elliptic instabilities is done on a mesh that permits amplification of several axial wavelengths. The axial extent of the domain corresponds to 2.1 chords. Figure 3

shows iso-contours of vorticity for different stages of the instability development. Image 1) shows the linear stage of instability, 2) the final amplitude of the axial wavelength at the end of the linear instability phase. 3) shows the vortex deformation in the late stage of the weakly non-linear phase, and 4) the non-linear saturation of the perturbed vortex.

a) b)

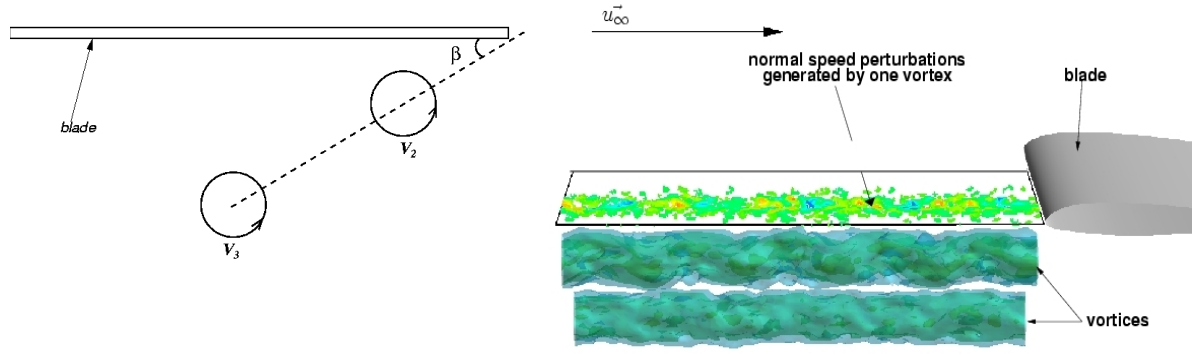

Figure 4: a) schematic representation of blade vortex-pair interaction. b) exemple of extracted gust plane.

To determine blade pressure fluctuations, a 2D plane is extracted from the 3D CFD computation domain. Only the normal component of the velocity field as regards to this plane is considered. Actually Amiet's theory enables to compute the aerodynamic response of a flat plate airfoil to this 2-dimensional gust (see Figure 4b). The 2D plane is extracted considering a constant interaction angle β and constant mis-distance md between the blade and the corotative vortex pair (see Figure 4a)). The extent of the extracted plane in the spanwise direction correspond to 5% of the blade span.

3.2 Blade pressure fluctuations

In order to determine the pressure perturbations resulting from the incident velocity perturbation that the blade would see when passing near the perturbed vortex, we use Amiet's theory. One considers that the gust obtained by the procedure presented before is carried by a free stream velocity $U_{inf}=\Omega R+U_{av}sin(\psi)$ where Ω is the angular velocity of the rotor, R the normalised span coordinate, U_{av} the advancing speed and ψ the angle between the span direction and the advancing speed vector. In this approach, spanwise position and interaction angle γ between blade and vortex axis are taken into account. Values of γ, β, md are deduced from ONERA BVI computation chain. In the following, the x axis is oriented in the chordwise direction, and y in the spanwise direction. The x coordinates are normalised by the half-chord and varies between -1 and 1.

For a normal velocity perturbation of wave number vector $\vec{k}=(k_x,k_y)$ normalised by the half chord $c/2$, assuming that free-stream angle of attack is null, Amiet [18] defined the local pressure jump ΔP across the airfoil as :

$$\Delta p(\vec{k},t,x)=2\pi\rho_o A(\vec{k})\,g(x,\vec{k},M)\,e^{i(k_y y-k_x W_0 t)} \tag{3.1}$$

Where $A(\vec{k})$ is the amplitude associated to the wave number vector $\vec{k}$, ρ_0 is the density, and

g the local transfer function between incident velocity and airfoil pressure jump. Lift coefficient are obtained by integrating the pressure forces over the chord and summing the contributions of all wave numbers.

$$c_z(t)=\frac{2}{\rho U_{inf}^2}\int_{-\infty}^{+\infty}\int_{-1}^{1}\Delta p(\vec{k},x,t)\,dx\,d\vec{k} \quad (2) \tag{3.2}$$

For high frequencies, if the gust/airfoil intersection moves supersonically relative to the fluid, the profile response function has been given by Amiet as :

$$g(x,\vec{k},M)=g_1(x,\vec{k},M)\left(1+\frac{\sqrt{1+x}}{2}\left[(1+i)E\left(2\frac{k_x}{1-M^2}M_\infty(1-x)-1\right)\right]\right) \tag{3.3}$$

With $M_\infty=\sqrt{(M^2-(1-M^2)\frac{k_x^2}{k_y^2})}$, $E(x)=\frac{1}{\sqrt{(2\pi)}}\int_0^x\frac{e^{-i\xi}}{\sqrt{(\xi)}}d\xi$. g_1 is defined as :

$$g_1(x,k_x,k_y)=\frac{1}{\pi\sqrt{(\pi(1+M)K_x(1+x))}}e^{-i\frac{k_x}{(1-M^2)}(M_\infty(1+x)-M^2x-1)+\pi/4} \tag{3.4}$$

Burley [19] examined the experimental pressure jump spectra of HART II test for different chordwise sensor locations in the azimuthal domain where BWI occurs. She remarked that the fall-off in spectral response is similar for all the values of x/c. This property tends to show that chordwise pressure distribution can be expressed as a function of x, and is independent of the gust wave-number. Thus, it seems that the chordwise pressure distribution proposed by Amiet is not adapted to our case. Indeed, Amiet's theory assumes that the distribution of pressure perturbations in the chordwise direction depends on the considered wave-number. For this reason, in the following, we will only consider the section lift coefficient obtained by Amiet's theory.

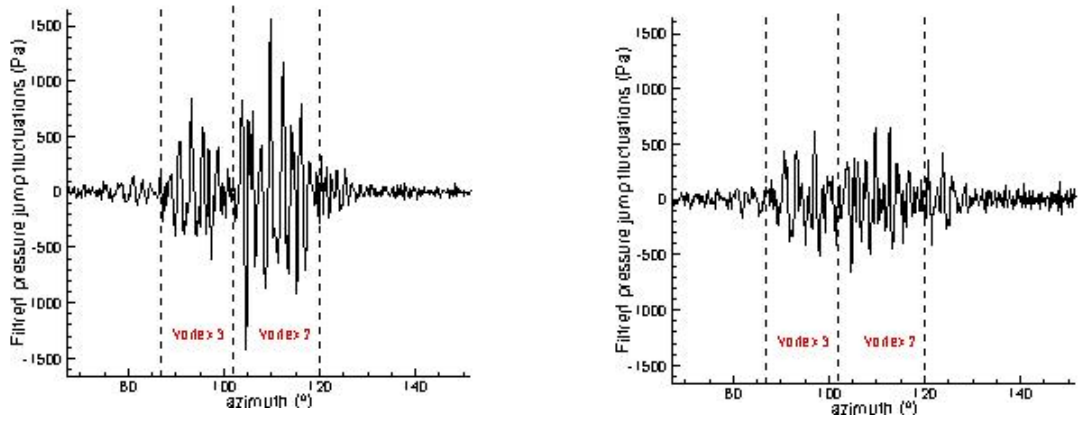

Figure 5: Typical experimental high-pass filtered blade pressure as a function of azimuth for r/R=0.87, left:3% chord. right: 6% chord

Nevertheless, when considering a high-frequency gust encountering an airfoil, it is well known

that compact chordwise approximation is not adapted for acoustic calculation. For this reason we need a chordwise pressure distribution function. We thus tried to define a function f to distribute along the chord the lift coefficient obtained from Amiet's theory. We looked for a continuous and integrable function that will advantage the lift of the leading edge and will decrease as x increases, as in the stationary case. We evaluate the decrement of function f from experimental HART II data at densely instrumented blade sections. An example of experimental signal from HART II corresponding to pressure for blade Section r/R=0.87 at 3% and 6% chord transducer locations is provided in Figure 5. The figure shows high-variance pressure fluctuations related to the two oblique blade-vortex interaction with Vortex 2 and Vortex 3 defined in Figure 1.

The RMS value of this signal P_{xc}, where xc is the normalised chord coordinate, of this signal is then evaluated in each azimuthal window corresponding to interactions. For example, considering the windows associated to blade/Vortex 2 interaction result gives ratio $P_{0.06}/P_{0.03}=0.48$ and $P_{0.1}/P_{0.03}=0.35$. Results are similar for the window associated to Vortex 3. From these information, we deduce the chordwise pressure jump distribution function f :

$$f(x)=\frac{1}{k}\frac{(1-e^{-\alpha\frac{xc^2}{0.02}})}{xc} \tag{3.5}$$

Where $\alpha=\sqrt{1.256}$ is a constant set to obtain a maximum value of f at xc=0.02 and k is the value of the integral of f over the chord. Consequently, the pressure coefficient will be distributed over the chord as follows :

$$\Delta c_p(x)=c_z f(x) \tag{3.6}$$

$\Delta c_p(x)$ being the pressure jump coefficient and c_z the lift coefficient.

3.3 Results

In this section we describe the procedure employed to compute the blade pressure jump and present the results. We then compare the results of noise loading computations performed with compact chordwise approximation and chordwise distributed sources.

In the following, we have considered two different interactions of the blade with perturbed vortices. The relative interaction configurations are deduced from the wake geometry presented in Figure 1. The gust is extracted from the numerical simulation at a time corresponding to the end of the linear regime. The β angle representing the angle between the plane joining the two vortices and the blade spanwise direction has a major influence. Indeed, the axial deformation due to elliptical instability grows in a preferential direction. In our study we choose to determine β from a free-wake computation. Thus, this angle will not be adjusted to obtain maximum pressure jump amplitude. The azimuthal range D on which pressure jump fluctuations will be imposed is D=[90°,130°]. We thus choose to set beta as the average angle value obtained from the wake computation in the azimuthal domain D. We found $\beta=7°$. The constant distance md related to the blade-Vortex 2 mis-distance is set to $md=2\text{cm}$. Finally, the gust-airfoil angle of interaction is set to 10° for Vortex 2, and 15° for Vortex 3.

Figure 11 presents the time history of pressure jump fluctuations for a spanwise coordinate r/R=0.87. The pressure jump perturbations are obtained from Amiet's lift coefficient distributed along the chord according to the function f. The first hundred harmonics have been removed. The amplitude of the fluctuations associated to Vortex 2 are weaker than the ones found from

experimental data presented in Figure 5. We can notice that the azimuthal domain of the pressure fluctuations associated to Vortex 2 is similar to the one observed in experiment. Differently the azimuthal domain of the pressure fluctuations associated to Vortex 3 is smaller. This point could be explained by the hypothesis of constant angle of interaction γ . Another remark can be done by comparing the average amplitude of the two interactions. Unlike what has been observed on experimental data, the average pressure fluctuation amplitude associated to blade-Vortex 3 interaction is more intense than the average pressure fluctuation amplitude of blade-Vortex 2 interaction. This can be explained by the fact that mis-distances between the blade and Vortex 2 and Vortex 3 are roughly equal in our computations while experiment suggests a larger mis-distance between the blade and Vortex 3 than with Vortex 2.

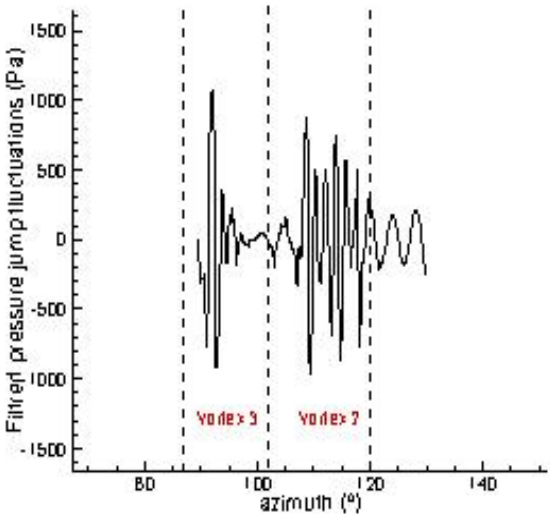

Figure 6: computational pressure jump fluctuations associated to blade/vortex interaction at r/R=0.87 .

Figures 7, 8, 9, 10 show predicted noise footprints using PARIS for different computations. The microphone layout is situated in a horizontal plane at 1.2 rotor radius under the rotor. Noise levels are expressed in dB filtered between 43 and 73 bpf (blade passage frequency). Figures 7 and 8 show the noise footprint associated to blade interaction with Vortex 2. Figure 7 is issued from a computation performed with compact chordwise approximation and Figure 8 from a computation using distributed sources in the chordwise direction. As expected, compact chordwise approximation has an influence on directivity and noise level. Indeed, the maximum noise zone is situated upstream of the rotor disk when considering compact sources and on the right of the rotor disk when considering distributed sources. Moreover maximum noise level is higher in the case of computation from compact sources (89.7 dB) than with distributed sources (87.7 dB).

Figure 9 shows the noise footprint associated to blade interaction with Vortex 3. We notice a maximum noise level of 89.1dB and a maximum noise zone situated more inboard of the rotor disk than in the case of interaction with Vortex 2.

Finally, Figure 10 presents the noise footprint obtained from a computation where the interactions between the blade and the two vortices are considered. The relative good agreement in noise level between experiment (presented in Figure 11) and our computation may be considered fortuitous as regards to the lack of accuracy in the determination of interaction parameters. Which makes mores sense, however, is the good agreement in directivity between computation and experiment.

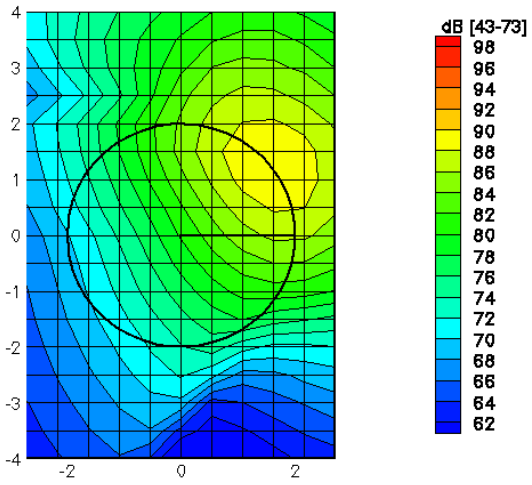

Figure 7 : computed noise footprint related to blade/Vortex 2 interaction obtained with compact chordwise approximation.

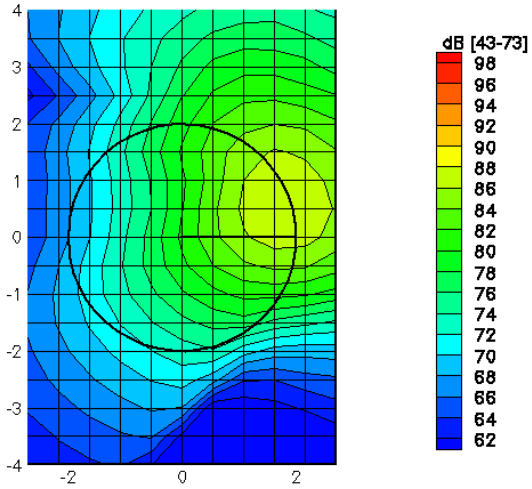

Figure 8 : computed noise footprint related to blade/Vortex 2 interaction obtained from distribution of the lift.

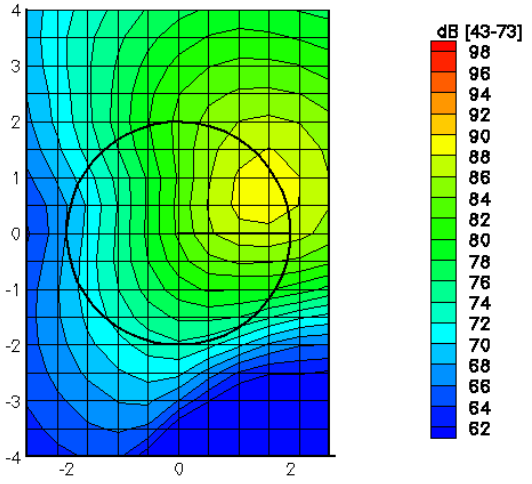

Figure 9 : computed noise footprint related to blade/Vortex 3 interaction obtained from distribution of the lift.

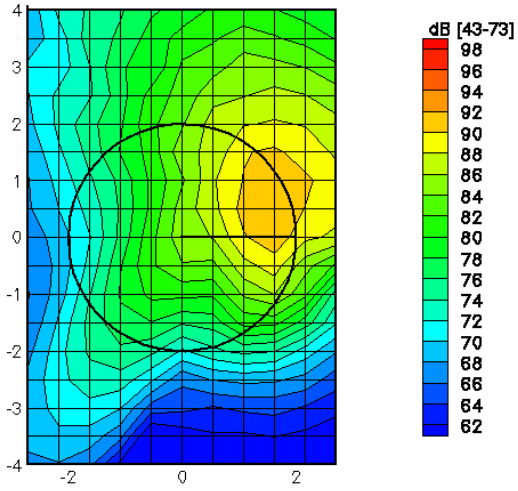

Figure 10 : noise footprint related to blade/Vortex 2 and blade/Vortex 3 interactions obtained from distribution of the lift.

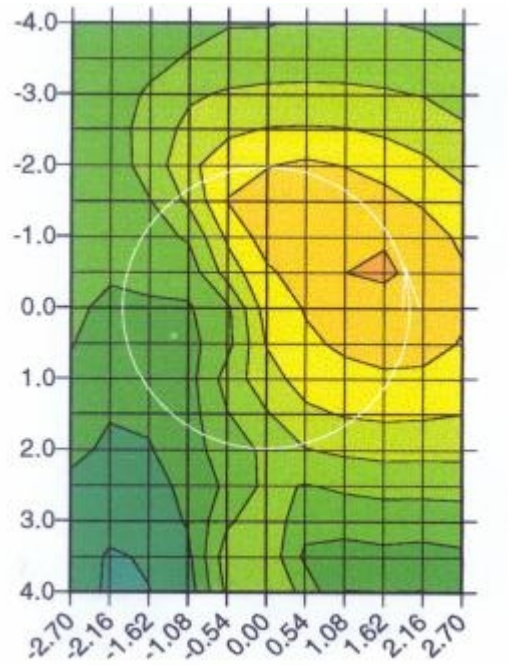

Figure 11: experimental noise contours of BWI for climbing flight configuration. (Average spectrum filtered between 3Khz and 6,5 Khz)

4 CONCLUSION

A CFD simulation of short wave instabilities that may occur on helicopter rotor tip vortices has been performed for climb flight conditions in a simplified configuration of two analytical parallel rectilinear vortices. The instability mechanisms have been described and the influence of the parameters driving the instability growth rate has been discussed. A good agreement has been observed between numerical and theoretical linear growth rate.

Then the unsteady aerodynamic field provided by the numerical simulation has been used to compute the surface pressure response of rotor blades during a close encounter with such vortex instabilities in conditions where BWI noise occurs. For this, a 2D gust has been extracted from the CFD computation and the blade response has been deduced from compressible Amiet's theory. Comparable amplitudes have been observed between computed blade pressure fluctuations and corresponding HART II experimental results.

In the last part of the paper, these blade pressure fluctuations are used as input data for a loading noise calculation. The noise levels and directivity in a horizontal plane below the rotor are computed and compared to HART II experimental data. A good agreement in terms of noise levels and directivity is observed.

The results tend to show that interaction between rotor blades and vortices subject to elliptical instabilities is a good candidate mechanism to explain BWI generation. This support the hypothesis laid by Bouchet.

Nevertheless, our study presents some uncertainties that should be removed in the future.

As shown in this paper, elliptical instabilities expand in a preferential direction and their growth rate depends on the distance separating the two vortices. Thus the geometrical arrangement of the wake has a major importance in the instability development. The effect of a more realistic

configuration (pair of non parallel and non-uniform vortices) on the expansion of this kind of short-wave instabilities will be studied. Furthermore, since blade-vortex interaction parameters like mis-distance and angle of interaction are key parameters for noise production, a finer description of the wake is needed. It could be provided in the future thanks to CFD progress.

Acknowledgements

The authors would like to acknowledge Guillaume Perez for his participation in this study.

Bibliography

[1] T.F. Brooks, J. R. Jolly, M.A.Marcolini , "Helicopter Main-Rotor Noise.", NASA Technical Paper, n°2825 (1988).
[2] J. Brezillon, J. Prieur, G. Rahier, "Investigation on Broadband Helicopter Rotor Noise.", AHS Rotorcraft Acoustics and Aerodynamics Specialists Meeting, Williamsburg, Virginia, Oct 1997.
[3] W.R Splettstoesser, R. Kube, W. Wagner, U. Seelhorst, A. Boutier, F. Micheli, E. Mercker, K. Pengel, "Key Results from a Higher Harmonic Control Aeroacoustic Rotor Test (HART)", Journal of the AHS, 1997,42(1).
[4] S.A.L Glegg, "The Prediction of Blade Wake Interaction Noise Based on a Turbulent Vortex Model", 12th AIAA Aero-Acoustics Conference. San Antonio, Texas, 1989.
[5] K. S. Wittmer, W. J. Devenport, S. A. L. Glegg , "Perpendicular Blade Vortex Interaction.", AIAA Journal, Sept 1995, pp.1667-1674
[6] S. A. L. Glegg, S. Witmmer J. Devenport, D. S. Pope, "Broadband Helicopter Noise", AHS Specialists' Meeting for Rotorcraft Acoustic and Aerodynamics, Williamsburg, Virginia, Oct 1997.
[7] E. Bouchet, G. Rahier, "Structure of the Blade Pressure Fluctuations Generated by Helicopter Rotor Blade-Wake Interaction", 56th AHS Annual Forum, Virginia Beach, Virginia, may 2000.
[8] S. Le Dizes, F. Laporte, "Theoretical Predictions for Elliptical Instability in a Two Vortex Flow.", J. Fluid Mech, 2002, pp.169-201
[9] F. Laporte, A. Corjon, "Direct Numerical Simulations of the Elliptic Instability of a Vortex Pair", Phys. Fluids, 2000, pp.1016-1031
[10] Gazaix, M., Jolles, A., and Lazareff, M., "The elsA Object-Oriented Computational Tool for Industrials Applications", 23rd Congress of ICAS, Toronto, Canada, September 2002.
[11] Amiet R.K., "High Frequency Thin-Airfoil Theory for Subsonic Flow.", AIAA journal, 1976, pp.1076-1082
[12] P. Spiegel, "Prévision et Analyse du Bruit Emis par un Rotor Principal d' Hélicoptère en Présence d' Interactions Pale-Tourbillon (Prediction and Analysis of Blade-Vortex Interaction Noise from a Helicopter Main Rotor)",Doctorate Thesis, Université du Maine, ONERA Publication no 1996-1 , July 1995.
[13] B. Van der Wall, B. Junker, M., Raffel, H. Richard, W. Wagner, C., L., Burley, T., F., Brooks, Y., H., Yu, C. Tung, E., Mercker, K. Pengel, H., Holthusen, Ph. Beaumier, Y. Delrieux., "The HART-II Test in the LLF of DNW – A Major Step Towards Rotor Wake Understanding.", 28th European Rotorcraft Forum, Bristol, UK, September 2002.
[14] Y. O. Han, J. G. Leishman, A. J. Coyne, "On the Turbulent Structure of a Tip Vortex Generated by a Rotor ", 52th Annual Forum Proceedings, Washington, DC, June 4-6 1996.
[15] K. W. McAlister, "Rotor Wake Development During the First Revolution", AHS 59th Annual Forum , Phoenix, Arizona, May 6-8 2003.

[16] G. Rahier, Y. Delrieux, "Blade Vortex Interaction Noise Prediction Using a Rotor Wake Roll-up Model", Journal of Aircraft, 1997, pp.29-41
[17] D. Sipp, "Weakly Nonlinear Saturation of Short Wave Instabilities in a Strained Lamb-Oseen Vortex", Physics of Fluids, 2000, pp.1715-1729
[18] R. K. Amiet, "Noise Produced by Turbulent Flow Into a Rotor : Theory Manual for Noise Calculation", NASA-CR-181788 , n° (1989).
[19] C. L. Burley, T. F. Brooks, W. R. Splettstoesser, K.-J. Schultz, R. Kube, H. Bucholtz, "Blade-Wake Interaction Noise fopr a BO-105 Model Main Rotor", AHS Specialists' Meeting for Rotorcraft Acoustic and Aerodynamics, Williamsburg, Virginia, Oct 1997.